
BAYES-PROBE: Distribution-Guided Sampling for Prediction Level Sets

Serena Booth^{*1} Yilun Zhou^{*1} Ankit Shah¹ Julie Shah¹

Abstract

Building machine learning models requires a suite of tools for interpretation, understanding, and debugging. Many existing methods have been proposed, but it can still be difficult to probe for examples which communicate model behaviour. We introduce BAYES-PROBE, a model inspection method for analyzing neural networks by generating distribution-conforming examples of known prediction confidence. By selecting appropriate distributions and confidence prediction values, BAYES-PROBE can be used to synthesize ambivalent predictions, uncover in-distribution adversarial examples, and understand novel-class extrapolation and domain adaptation behaviours. BAYES-PROBE is model agnostic, requiring only a data generator and classifier prediction. We use BAYES-PROBE to analyze models trained on both procedurally-generated data (CLEVR) and organic data (MNIST and Fashion-MNIST). Code is available at <https://github.com/serenabooth/Bayes-Probe>.

1 Introduction

Debugging, interpreting, and understanding neural networks can be challenging (Odena et al., 2019; Lipton, 2018; Doshi-Velez & Kim, 2017). Previous interpretability methods include saliency maps (Zeiler & Fergus, 2014; Simonyan et al., 2013), input perturbations (Ribeiro et al., 2016; Lundberg & Lee, 2017), prototype anchoring (Kim et al., 2014; Li et al., 2018b; Chen et al., 2019), tracing with influence functions (Koh & Liang, 2017), and concept quantification in classification (Ghorbani et al., 2019b; Kim et al., 2017). Some methods provide ‘local’ explanations by justifying decisions for specific inputs. Other methods focus on understanding intermediary components of trained neural

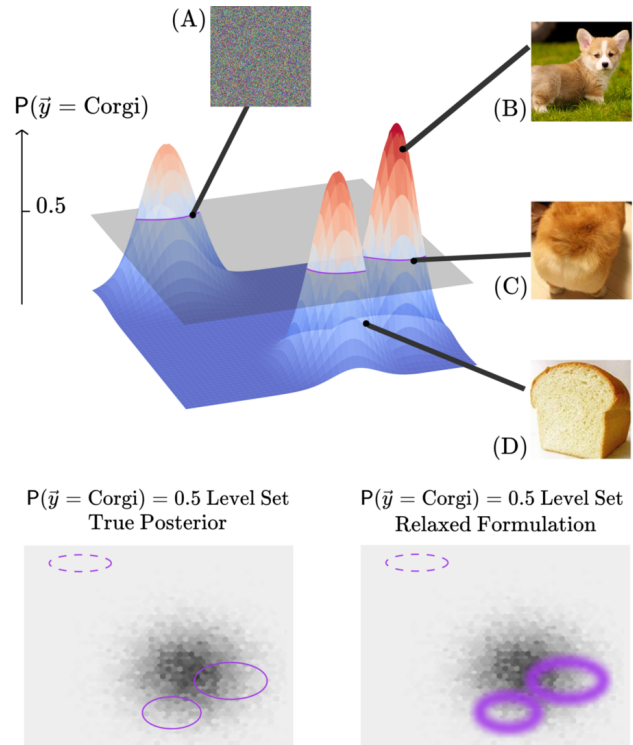


Figure 1: An overview of our distribution-probing method. Given a Corgi/Bread classifier and a generative model for the data, we generate *prediction level sets*, or sets of examples of target prediction confidence. (A) Existing adversarial approaches can perturb a given image to the target prediction confidence (e.g. $p_{\text{corgi}} = p_{\text{bread}} = 0.5$); however, such examples are out of the data distribution. (B, C, D) BAYES-PROBE, on the other hand, takes in the data distribution and samples from the target prediction level set (e.g., likely Corgi, likely Bread, or ambivalent between Corgi and Bread). Bottom left: by overlaying the classifier level set of ($p_{\text{corgi}} = p_{\text{bread}} = 0.5$) over the data distribution (the black heatmap), we note example (A) is not sampled because its likelihood is extremely low under the generative model, while example (C) will be sampled because it is likely under the generative distribution. Bottom right: As sampling directly from the true posterior is infeasible, we introduce a relaxed formulation to sample from the “widened” level set.

^{*}Equal contribution ¹Computer Science and Artificial Intelligence Laboratory, Massachusetts Institute of Technology. Correspondence to: Serena Booth <serenabooth@csail.mit.edu>, Yilun Zhou <yilun@csail.mit.edu>.

networks, like convolutional layers (Bau et al., 2017; Olah et al., 2017). These techniques have been used successfully to understand and improve models (Zeiler & Fergus, 2014), but care must be taken not to provide misleading insights and explanations (Kindermans et al., 2019; Adebayo et al., 2018; Rudin, 2019) and to consider the risk of adversarial attacks (Slack et al., 2019; Ghorbani et al., 2019a).

To complement this suite of available interpretability tools, we propose BAYES-PROBE: a method to gain insight into model behaviours by probing for examples. BAYES-PROBE inspects a model by sampling data at known prediction confidence, e.g., $p_1 = 0.7$, $p_0 = 0.3$ for a binary classifier. We call these *prediction level sets*. Given a data distribution and a trained classifier, BAYES-PROBE samples examples with a specified prediction from the posterior of a hierarchical Bayesian model by applying Markov Chain Monte-Carlo (MCMC) inference methods. We implement this inference through probabilistic programming (Cusumano-Towner et al., 2019). We demonstrate BAYES-PROBE on CLEVR, a procedurally-generated visual question answering dataset (Johnson et al., 2017), MNIST, and Fashion-MNIST (Xiao et al., 2017). For each dataset, we demonstrate how BAYES-PROBE can aid model inspection with several use cases. Using BAYES-PROBE, we find ambiguous examples and expose highly-confident in-distribution adversarial examples. We further demonstrate model fragility in the presence of novel classes. Lastly, we show that a domain-adapted model can become increasingly prone to the problem of overconfidence.

2 Related Work

2.1 Model Explanation and Inspection

Model inspection techniques aim to expose model vulnerabilities, support model debugging, and enable human users to develop understanding of model behaviours. Zeiler & Fergus (2014) introduced a technique to interpret intermediate feature layers of neural network classifiers; this technique works by visualizing the classification score drop when occluding an image at fixed regions. Zeiler & Fergus (2014) further demonstrated how these activation visualizations could be used for model diagnosis and subsequently inform better model design. Simonyan et al. (2013) created the generalized form of this analysis technique: saliency maps. While saliency maps have become ubiquitous tools for interpreting neural networks, these visualizations can be misleading. Saliency methods can produce reasonable outputs, even when produced with networks with randomized weights (Kindermans et al., 2019; Adebayo et al., 2018).

LIME (Ribeiro et al., 2016) and SHAP (Lundberg & Lee, 2017) are post-hoc explanation techniques which perturb inputs and score how these perturbations affect classification. TCAV is an analogous method for scoring the relative

importance of concepts to a neural network’s classification (Ghorbani et al., 2019b; Kim et al., 2017). While these techniques can be useful for understanding how neural networks operate and process classification tasks, they are complementary to BAYES-PROBE. For example, TCAV can determine that stripes are an important concept when classifying zebras, but BAYES-PROBE can find that a model is unable to differentiate between striped zebras and striped skunks.

Model testing is an approach for debugging neural networks. Odena et al. (2019) introduced TensorFuzz, a testing suite which focuses on discovering errors on rare inputs. Like BAYES-PROBE, TensorFuzz uses mutations of inputs to explore the classification manifold; however, TensorFuzz mutations are selected to optimize for coverage. By design, these mutated inputs are not drawn from the test distribution. Several other neural network testing paradigms have been proposed (Wicker et al., 2018; Pei et al., 2017; Ma et al., 2018). The key difference between these network testing paradigms is in their respective goals. Network testing paradigms are typically searching for software failures—for example, numerical errors. BAYES-PROBE instead searches for prediction level sets which can be used to better a user’s understanding of a model through inspection.

Finally, an alternative interpretability approach is policy summarization, in which a system produces overview explanations (Amir et al., 2019; Huang et al., 2019). Unlike other interpretability approaches, policy summarization aims only to give a high level intuition for how an agent or classifier may behave. One such policy summarization approach formulates a set cover problem over histories of system states to produce an overview of an agent’s behaviour (Hayes & Shah, 2017). BAYES-PROBE could be used alongside these techniques: instead of using hand-defined predicates as the explanation medium, BAYES-PROBE could be used to provide prediction level sets as the explanation medium.

2.2 Confidence in Neural Networks

BAYES-PROBE explores confidence level sets in neural networks. Guo et al. (2017) showed that many neural networks are over-confident, with many incorrect predictions having undue high confidence. While many approaches aim to address this neural network overconfidence problem (e.g. Thulasidasan et al., 2019; Lee et al., 2017; Gal & Ghahramani, 2016; Blundell et al., 2015), our work is complementary to these efforts. Rather than altering the confidence of a neural network, BAYES-PROBE instead exposes examples with a particular confidence. As a result, if the model is overconfident, BAYES-PROBE may return few, if any, valid samples with ambivalent predictions. Meanwhile, BAYES-PROBE may find many misclassifications with very high confidence. As such, BAYES-PROBE can be used to assist in the diagnosis of overconfident networks.

3 Methodology

Given a classifier $f : X \rightarrow \Delta^L$ which maps a data point to the probability simplex of L classes, the overall goal is to find an input $\mathbf{x} \in X$ such that $f(\mathbf{x}) = \mathbf{p}$ for some particular prediction confidence $\mathbf{p} \in \Delta^L$. A common approach to achieve this starts with some initial guess \mathbf{x}_0 and uses a gradient-based method to iteratively optimize the function $\mathcal{L}(x) = d(f(\mathbf{x}), \mathbf{p})$, where $d(\cdot, \cdot)$ is some distance metric (for example, total variation distance). This method is used by most adversarial attacks; however, there is no guarantee the resulting sample will conform to a particular distribution. Consequently, defenses against adversarial attacks may rely on examples being out-of-distribution. For other model inspection use cases, out-of-distribution samples may not be helpful for interpreting or debugging a model (i.e., especially if the sample is seemingly composed of noise).

Instead, we introduce a data distribution $p(\mathbf{x})$ and consider the inference problem of sampling from the posterior

$$p(\mathbf{x}|f(\mathbf{x}) = \mathbf{p}) \propto p(\mathbf{x})p(f(\mathbf{x}) = \mathbf{p}|\mathbf{x}). \quad (1)$$

Unfortunately, solving this exactly is infeasible because in general the set $\{\mathbf{x} : f(\mathbf{x}) = \mathbf{p}\}$ has measure 0. To mitigate this problem, we relax the formulation by “accepting” \mathbf{x} when $f(\mathbf{x})$ is close to \mathbf{p} , as shown in Figure 1. We introduce a random variable (or vector) u , with the conditional distribution $u|\mathbf{x} \sim q(f(\mathbf{x}))$, and its target u^* , such that

$$\mathbb{E}_q[u|\mathbf{x}] = u^* \implies f(\mathbf{x}) = \mathbf{p}. \quad (2)$$

We now need to sample from the new posterior

$$p(\mathbf{x}|u = u^*) \propto p(\mathbf{x})p(u = u^*|\mathbf{x}). \quad (3)$$

When the sampled data has high probability, the classifier prediction will closely match \mathbf{p} under expectation.

We consider three probability assignments of \mathbf{p} :

$\mathbf{p}_i = 1, \mathbf{p}_{-i} = 0$: The classifier should be as confident in its class i prediction as possible. This is useful for visualizing highly confident examples (which can be classified correctly, incorrectly, or out-of-distribution). For this case:

$$u|\mathbf{x} \sim \text{No}(f(\mathbf{x})_i, \sigma^2), \quad (4)$$

$$u^* = 1, \quad (5)$$

where σ is a hyper-parameter.

$\mathbf{p}_i = \mathbf{p}_j = 0.5, \mathbf{p}_{-i,j} = 0$: The classifier should be equally ambivalent between class i and class j , while not predicting any other classes. This is useful for visualizing examples on a decision boundary. For this case:

$$u_1|\mathbf{x} \sim \text{No}(|f(\mathbf{x})_i - f(\mathbf{x})_j|, \sigma_1^2), \quad (6)$$

$$u_2|\mathbf{x} \sim \text{No}(\min(f(\mathbf{x})_i, f(\mathbf{x})_j) - \max_{k \neq i,j} f(\mathbf{x})_k, \sigma_2^2), \quad (7)$$

$$u_1^* = 0, \quad (8)$$

$$u_2^* = 0.5, \quad (9)$$

where we can write $\mathbf{u} = [u_1, u_2]^T$, $\mathbf{u}^* = [0, 0.5]^T$ for notation consistency, and σ_1, σ_2 are hyper-parameters.

$\mathbf{p} = \mathbf{p}^*$: The samples conform to any given confidence target \mathbf{p}^* . This is the most general case. For this case:

$$u_i|\mathbf{x} \sim \text{No}(f(\mathbf{x})_i, \sigma^2), \quad (10)$$

$$u_i^* = \mathbf{p}_i^*, \quad (11)$$

where σ is a hyper-parameter.

Rather than sampling directly from the data distribution, we sample in the latent factor space Z , which is mapped to X via a deterministic reconstruction function $g : Z \rightarrow X$. If, for example, our generative model is learned by a GAN or a VAE, the latent distribution $p(\mathbf{z})$ is a unit Gaussian.

To summarize, given

$$\mathbf{z} \sim p(\mathbf{z}), \quad (12)$$

$$\mathbf{x} = g(\mathbf{z}), \quad (13)$$

$$u|\mathbf{z} \sim q(f(g(\mathbf{z}))), \quad (14)$$

$$p(\mathbf{z}|u = u^*) \propto p(\mathbf{z})p(u = u^*|\mathbf{z}), \quad (15)$$

we wish to sample from Eqn 15 and reconstruct $\mathbf{x} = g(\mathbf{z})$.

We use two Markov Chain Monte Carlo (MCMC) inference methods for sampling from the posterior: Metropolis-Hastings and Hamiltonian Monte Carlo. In our experiments, we use Metropolis-Hastings when the prediction is not differentiable with respect to \mathbf{z} (e.g., when rendering is non-differentiable). Otherwise, we use Hamiltonian Monte Carlo as the inference procedure. For the Hamiltonian Monte Carlo method, we use the No-U-Turn sampler (Hoffman & Gelman, 2014; Neal et al., 2011) and the probabilistic programming language Pyro for implementation (Bingham et al., 2018). σ is chosen to be 0.05 for all experiments.

4 Experiments

4.1 Experiment Overview

BAYES-PROBE enables the evaluation of a classifier on a target generative distribution \mathbb{P}_G irrespective of the distribution of the classifier training set \mathbb{P}_C . We demonstrate the versatility of BAYES-PROBE on four relationships between \mathbb{P}_G and \mathbb{P}_C , as illustrated in Figure 2.

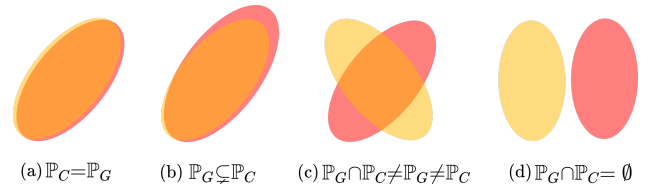


Figure 2: Evaluated relations between classifier training data (\mathbb{P}_C , red) and generator training data (\mathbb{P}_G , yellow). (a) \mathbb{P}_C and \mathbb{P}_G are identical. (b) Support of \mathbb{P}_G is a strict subset of \mathbb{P}_C . (c) \mathbb{P}_G and \mathbb{P}_C are partially overlapping. (d) \mathbb{P}_C and \mathbb{P}_G have disjoint supports.

First, in Section 4.3, 4.4 and 4.5, we consider $\mathbb{P}_C = \mathbb{P}_G$ (Figure 2(a)). This case allows us to find examples which conform to the training data distribution and achieve highly confident or ambivalent predictions for target class(es).

In Section 4.6, we consider \mathbb{P}_C with narrower support than \mathbb{P}_G (Figure 2(b)). Specifically, \mathbb{P}_G excludes data in \mathbb{P}_C with a particular label. In this case, posterior sampling with P_G as the generative distribution can reveal whether there exist in-distribution adversarial examples.

Finally, in Section 4.7 and 4.8, we consider \mathbb{P}_C and \mathbb{P}_G with overlapping or disjoint supports (Figure 2(c) and (d)). We seek to understand how a classifier extrapolates to novel classes and how its performance degrades under domain adaptation (i.e., covariate shift).

4.2 Datasets

We evaluate our method on both procedurally-defined data (CLEVR) and natural data (MNIST and Fashion-MNIST).

CLEVR (Johnson et al., 2017) is a dataset and modeling environment which supports visual question answering. CLEVR is modeled as a 32-class classification problem, with classes ranging from yes/no answers to properties (e.g., colour, size) to numerical counts. In all our CLEVR experiments, we use the pre-trained model distributed by the original authors. Since the rendering program is not differentiable, we use the Metropolis-Hastings algorithm to perform sampling. Probabilistic programming allows us to readily employ custom proposal distributions tailored to our priors, and the proposal is Gaussian for the continuous variables (e.g., x-position) and categorical for the discrete variables (e.g., color), with a high probability for the current value and uniform low probabilities for the other values.

For MNIST and Fashion-MNIST, we train and use both VAE and GAN models as the generative process. For all use cases except domain adaptation, we train our own classifiers. For the domain adaptation analysis, we used the adversarial discriminative domain adaptation (ADDA) model (Tzeng et al., 2017) and the code provided by the authors to train both the baseline and the ADDA model. Further details on network architectures and additional samples are in the supplemental material.

4.3 High Confidence

We first evaluate BAYES-PROBE by finding highly confident examples. We infer highly confident scenes containing 5 spheres and 2 blue spheres, and every class for MNIST and Fashion-MNIST. Samples are shown in Figure 3.

4.4 Ambivalent Confidence

We then find examples where the neural network is ambivalent between two classes and is confident these samples should not be classified as any other class. We use a trained VAE model as our image distributions for MNIST

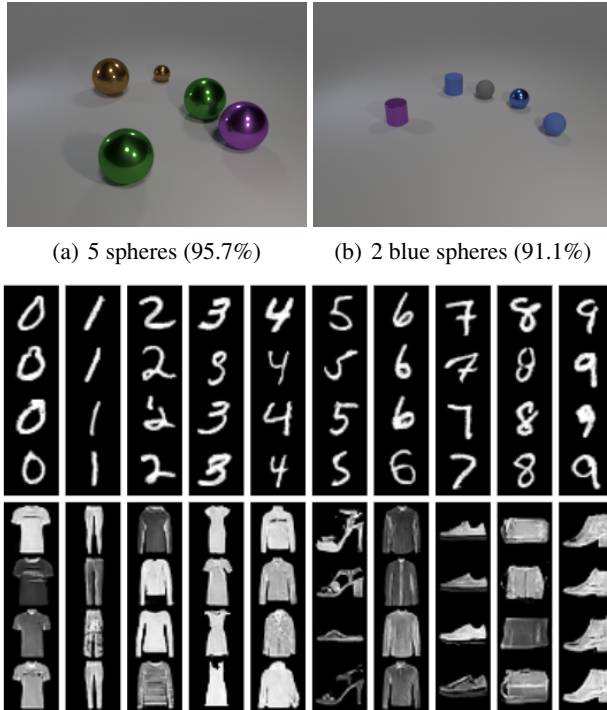


Figure 3: Inferred high classification samples for CLEVR (top), MNIST (middle), and Fashion-MNIST (bottom). There are no misclassifications. Fashion-MNIST columns represent T-shirt, trousers, pullover, dress, coat, sandal, shirt, sneaker, bag, and ankle boot, respectively.

and Fashion-MNIST. Figure 4 presents one sampled image for each pair of classes (e.g., Digit 1 vs. Digit 7; T-shirt vs. Pullover). Each entry of the matrix shows an ambivalent example for the two classes on its row and column boundary. As is expected, not all pairs result in successful sampling—for example, we were unable to find an ambivalent character with equal prediction confidence between a 7 and a 0. Figure 5 presents additional details for two pairs, Digit 1 vs. Digit 7 from MNIST and T-shirt vs. Pullover from Fashion-MNIST. The violin plot confirms that the neural network is indeed making the target predictions, and the latent visualization indicates that the samples lie around the class boundaries and are in-distribution (i.e., having close proximity to others from the prior in the latent visualization with T-SNE (Maaten & Hinton, 2008) dimensionality reduction). Note that these samples are ambivalent from the perspective of the classifier; some may be readily classified by a human.

4.5 Graded Confidence

BAYES-PROBE can also sample with confidence predictions which interpolate between classes. In Figure 6, we show MNIST samples which interpolate from ($\mathbf{p}_8 = 1.0, \mathbf{p}_9 = 0.0$) to ($\mathbf{p}_8 = 0.0, \mathbf{p}_9 = 1.0$) and Fashion-MNIST samples from ($\mathbf{p}_{\text{T-shirt}} = 1.0, \mathbf{p}_{\text{Trousers}} = 0.0$) to ($\mathbf{p}_{\text{T-shirt}} = 0.0, \mathbf{p}_{\text{Trousers}} = 1.0$), using a VAE as the generator. The target probability for other classes is 0.



Figure 4: Pairwise-ambivalent examples for MNIST and Fashion-MNIST classes. Each entry of the matrix shows an ambivalent example for the two classes on its row and column. Blacked-out cells indicate sampling failures. See Figure 5 for more samples and representative violin plots.

By interpolating between two quite different classes, we can gain some insight into the model’s behaviour. For example, in Figure 6, we see that the interpolation from 8 to 9 generally shrinks the bottom circle toward a stroke, which is the key difference between digits 8 and 9 to be the width of the bottom circle. For Fashion-MNIST, we consider the case of T-shirt vs. Trousers. We uncover that the presence of two legs is important for trousers classification, even appearing in samples with $(\mathbf{p}_{\text{T-shirt}} = 0.9, \mathbf{p}_{\text{Trousers}} = 0.1)$ (second column). In contrast, a wider top and the appearance of sleeves are important properties for T-shirt classification; most of the interpolated samples have a short sleeve on the top but two distinct legs on the bottom.

Empirically, for both ambivalent confidence (Section 4.4) and graded confidence (Section 4.5), sampling failed for most of the cases when using a GAN to model the data distribution. This may confirm the over-confidence problem noted by Guo et al. (2017), or suggest a shortcoming of our model, which is discussed in more detail in Section 5.

4.6 In-Distribution Adversarial Examples

Another application of BAYES-PROBE is to find in-distribution adversarial examples. Many previous approaches reveal that neural network predictions are locally unstable; i.e. an input can be slightly perturbed to make the network produce confident, incorrect predictions (Szegedy et al., 2013; Li et al., 2018a; Athalye et al., 2018; Carlini & Wagner, 2017; Nguyen et al., 2015; Goodfellow et al., 2014).

Such adversarial attacks produce examples that are out of distribution; indeed, a promising approach for detecting or defending against adversarial examples relies on these examples being out-of-distribution (Hendrycks & Gimpel, 2017; Etman et al., 2019). While common adversarial examples highlight how a classifier can fail in malicious environments, BAYES-PROBE exposes “in-distribution” adversarial examples (Gilmer et al., 2018) and highlights how realistic examples can also cause failures.

Specifically, if we train the classifier on the entire dataset, but we perform sampling with the data distribution induced by a generative model trained on data that are not from a particular class (Figure 2(b)), then the resulting samples can be considered adversarial examples for that class. For MNIST and Fashion-MNIST, we sample in-distribution adversarial examples for each class. Figure 7 depicts adversarial samples for each class in MNIST (top) and Fashion-MNIST (bottom). Upon inspection, we observe several interesting phenomena. For MNIST, some of the very thin 8s are classified as 1, stretched 9s are classified as 4, and a particular style of 2s and 3s are classified as 7. For Fashion-MNIST, most samples are between semantically similar classes, such as T-shirt \leftrightarrow shirt, and sneaker \leftrightarrow ankle boot. However, we also see that chunky shoes are likely to be classified as bags. We similarly expose in-distribution adversarial examples for CLEVR, as shown in Figure 8.

4.7 Novel-Class Extrapolation

Our model can be used to understand the extrapolation behaviours of a model when it encounters novel classes. While training and test distributions should ideally be the same, this assumption is often violated. One such violation occurs when a model encounters data from a new class. For example, if an autonomous driving system is trained on images of cars and pedestrians, it is desirable to know how such a model would behave when it sees a cyclist on the road. While many methods have been proposed to detect out-of-distribution data (Vernekar et al., 2019; DeVries & Taylor, 2018; Hendrycks & Gimpel, 2016; Liang et al., 2017), BAYES-PROBE facilitates model insight by revealing examples from novel classes that are likely to cause a false-positive detection, and can help further understand any inductive biases the model may have.

To evaluate the effect of data from novel classes on the CLEVR classifier, we consider the case of overlapping, non-equal support as in Figure 2(c). We use the pre-trained CLEVR classifier, which is only trained to classify cubes, cylinders, and spheres. We add a new shape, a cone, to the generator. For each target query, we revoke the generator’s ability to produce shapes of the given class. We demonstrate some inferred examples in Figure 9. Indeed, we find our inference method is consistently able to discover adversarial examples belonging to novel classes for each target class.

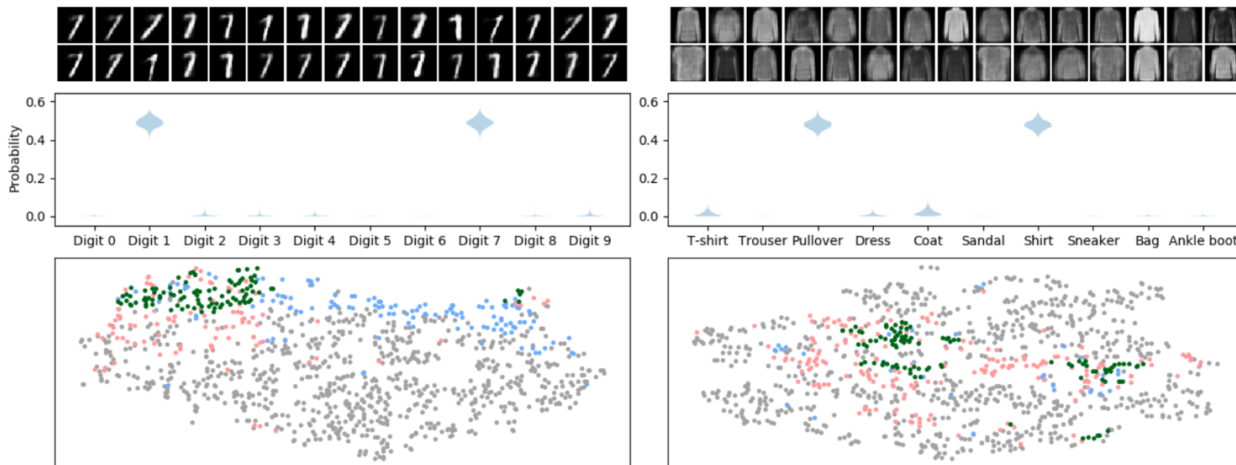


Figure 5: Left: ambivalent samples for digit 1 vs. 7 in MNIST. Right: ambivalent samples for pullover vs. shirt in Fashion-MNIST. Top: 30 sampled images. Middle: the ambivalent predictions made by the classifier. Bottom: latent space visualization. Green dots represent ambivalent samples from the posterior, red and blue dots represents samples from the prior that are predicted by the classifier to be either class of interest, and gray dots represents other samples from the prior. The ambivalent samples are on the class boundaries.

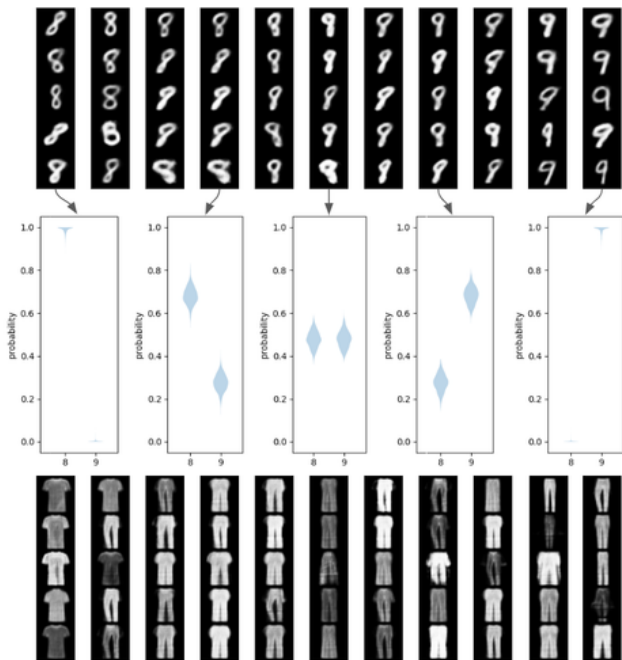


Figure 6: Confidence interpolation between digit 1 and 8 for MNIST, and between T-shirt and trousers for Fashion-MNIST. Each of the 11 columns show samples of confidence from [1.0, 0.0] to [0.0, 1.0], with interval of 0.1. Select confidence plots for MNIST samples are shown in the row.

To evaluate this extrapolation case on MNIST, we consider the case of disjoint classifier and generator support as in Figure 2(d). We split a dataset D into two disjoint parts, D_1 and D_2 , such that D_1 and D_2 only contain data with class labels in set C_1 and C_2 respectively, with $C_1 \cap C_2 = \emptyset$. Then we train a classifier on D_1 and a GAN generator on D_2 .

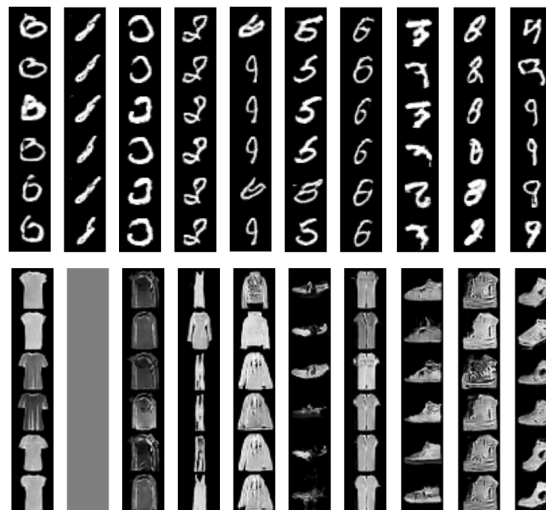
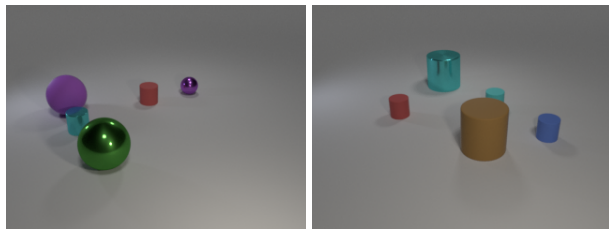


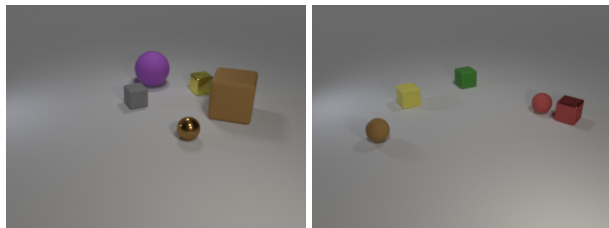
Figure 7: Adversarial examples for MNIST (top) and Fashion-MNIST (bottom). MNIST columns represent digit 0 to 9. Fashion-MNIST columns (left to right) represent T-shirt, trousers (failed to sample), pullover, dress, coat, sandal, shirt, sneaker, bag, and ankle boot. Despite the generator being unable to produce examples in the target class, most trials successfully find confident misclassifications.

We then sample high-confidence examples for each class in C_1 from the GAN-induced distribution. For MNIST, we choose $C_1 = \{0, 1, 3, 6, 9\}$, and $C_2 = \{2, 4, 5, 7, 8\}$. For Fashion-MNIST, we choose $C_1 = \{\text{Pullover, Dress, Sandal, Shirt, Ankle boot}\}$, and $C_2 = \{\text{T-shirt, Trousers, Coat, Sneaker, Bag}\}$. Figure 10 depicts samples from a GAN trained on D_2 for which the classifier trained on D_1 has high confidence for each class in C_1 .



(a) 1 Cube (99.7%)

(b) 1 Sphere (90.9%)



(c) 1 Cylinder (96.8%)

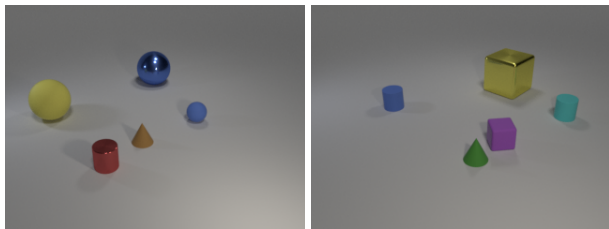
(d) 2 Cylinders (76.6%)

Figure 8: Adversarial examples for CLEVR. We revoke the generative model’s ability to produce objects of a target class (i.e., the generative model cannot produce cubes in 8(a)), and then infer examples of known high-confidence. 8(a) does not contain any cubes, but the pre-trained CLEVR classifier is 99.7% certain this scene contains 1 cube.

In Fashion-MNIST, some results are intuitive. For example, the only shoe class in set C_2 is “sneaker,” which accounts for most of the examples of “sandal” and “ankle boot” prediction, and the same goes for “coat” \rightarrow “pullover” and “T-shirt” \rightarrow “shirt.” Nevertheless, the classifier will also classify most of trousers as dresses, and bags of different styles will be classified as dresses, sandals, shirts, and ankle boots, despite visual dissimilarity. By comparison, for MNIST, it is hard to explain most of the samples. Several digits (e.g., 7) are inconsistently classified as different classes (i.e., split across 0, 1, and 9), likely because the digits are too visually distinct to allow for reasonable extrapolation.

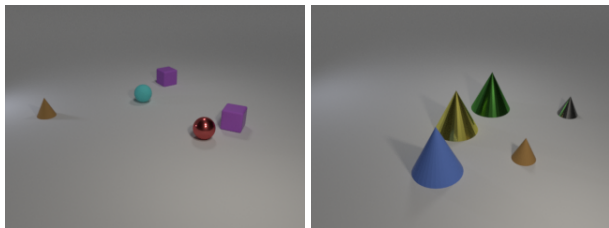
4.8 Domain Adaptation

Our model can also be used for domain adaptation analysis. Using BAYES-PROBE, we find the domain-adapted ADDA model can become increasingly prone to overconfidence. In domain adaptation, we have a source domain \mathcal{X}_S and a target domain \mathcal{X}_T , with shared label set C and cross-domain consistent decision rule $p(y|x)$ (Arjovsky et al., 2019; Long et al., 2015; Tzeng et al., 2014). The need for domain adaptation arises when the non-causal features vary across datasets. For example, for object recognition, lighting condition does not affect the object’s identity, and domain adaptation techniques can be applied to learn on bright images while being tested on dark ones. Domain adaptation is especially important in robotics, where algorithms trained in simulation often fail when using real sensor data in deployment (Peng et al., 2018; Tobin et al., 2017; Tan et al., 2018).



(a) 1 Cube (98.5%)

(b) 1 Sphere (92.7%)



(c) 1 Cylinder (97.7%)

(d) 5 Cubes (92.5%)

Figure 9: Extrapolation samples. We introduce a new shape—a cone—to the CLEVR generative model, and revoke the generative model’s ability to produce objects of a target class (i.e., the generative model cannot produce cubes in figure 9(a)), and then infer examples of known high-confidence. Figure 9(d) does not contain any cubes, but the pre-trained CLEVR classifier is 92.5% certain this scene contains 5 cubes.

To inspect a domain adaptation model, we sample high-confidence examples from the target domain for each class as predicted by the source-trained classifier. In our experiment, we trained the adversarial discriminative domain adaptation (ADDA) model (Tzeng et al., 2017) using the code provided by the authors without modification¹, with Street View House Number (SVHN) (Netzer et al., 2011) as the source domain and MNIST as the target domain. We also trained a baseline model with the same architecture on SVHN without the domain adaptation technique. Overall, we found that the baseline model achieves 61% target accuracy on MNIST, while the ADDA model achieves 71%.

But is this the whole story? To gain more insights, we sampled images from the MNIST data distribution with high prediction confidence for each class. Figure 11 presents samples from baseline model in the top row and ADDA model in the bottom row. The average confidence for the target class is over 99%. We can see both models have several wrong predictions. For example, some digit 6s are confidently classified as 4s by the baseline model, while some 0s are classified as 1s by the ADDA model. In addition, for each model and each target digit, we performed a human labeling on 10 images, and we check how many

¹<https://github.com/erictzeng/adda>. SVHN images are converted to gray-scale and 28×28 to match MNIST data.

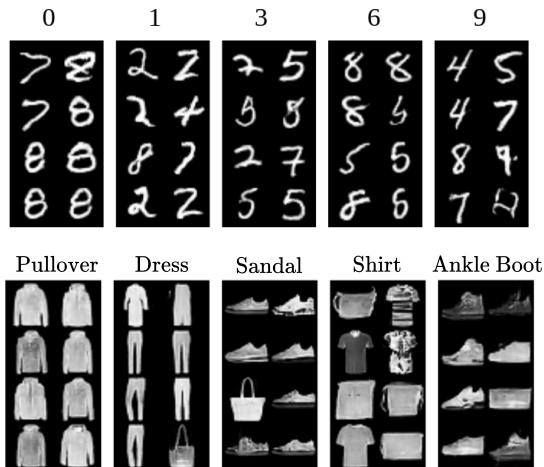


Figure 10: Highly confident OOD examples for different MNIST (top) and Fashion-MNIST (bottom) classes. Some Fashion-MNIST results are intuitive—for example, sneakers have been reclassified as sandals or ankle boots.

Table 1: Per-digit and aggregate accuracy among high confidence MNIST samples for the baseline and domain adjusted (ADDA) models. While the ADDA model has overall higher accuracy than the baseline (0.71 vs. 0.61), on high-confidence samples it has more misclassifications than the baseline (0.72 vs. 0.80), suggesting an overconfident model.

	0	1	2	3	4	5	6	7	8	9	Agg.
Baseline	1.0	0.6	1.0	0.7	0.5	0.9	0.9	0.7	1.0	0.7	0.80
ADDA	0.9	0.0	0.8	0.9	0.2	1.0	0.8	1.0	1.0	0.6	0.72

of those images are correctly labeled. The result is summarized in Table 1. Surprisingly, on high confidence samples, the baseline model is more accurate than the ADDA model. Although this does not fundamentally contradict the improved transfer performance for ADDA, this does highlight a concerning fact: ADDA seems to suffer from the over-confidence problem more severely, as a larger proportion of its high confidence samples are incorrect. In addition to allowing for fine-grained analysis beyond an aggregate accuracy, this analysis suggests the need for more extensive investigation into and potential calibration of confidence for domain adaptation models, which we leave to future work.

5 Discussion

The presented experimental results demonstrate the usefulness of BAYES-PROBE in gaining insights into trained black-box models by sampling data from appropriate posterior distributions. However, there are also some limitations of this method.

We discovered BAYES-PROBE cannot readily sample data with ambivalent predictions from a GAN prior; meanwhile, most ambivalent samples using a VAE prior appear blurry.



Figure 11: Highly confidence samples for each class (digit 0 to 9, in that order) of the baseline model (top) and ADDA model (bottom). BAYES-PROBE finds there to be more misclassified high-confidence examples with ADDA.

In general, GANs are trained to produce sharper images than VAEs due to the learned real/fake criterion. These observations suggest that either the classifier itself is not prone to ambivalent predictions (as in the over-confidence problem noted by (Guo et al., 2017)) or that our formulation is less effective at sampling ambivalent predictions as high confidence predictions. This question is further confounded by the lack of a general method to evaluate performance of inference algorithms on arbitrary models, and requires further empirical investigation.

Additionally, the current BAYES-PROBE formulation only works with classification models. Beyond classification, a new focus for deep learning is structured prediction. Further extending BAYES-PROBE to operate on these models would give the method enhanced analysis capabilities, e.g., for machine translation or style transfer models, but dependency among outputs must be explicitly taken into account.

6 Conclusion

We propose a model inspection method of sampling examples of known prediction confidence values. BAYES-PROBE selects examples such that the sampled data has high likelihood under a known data distribution. To achieve this, we use a Bayesian inference formulation and use probabilistic programming to sample from the posterior. On both procedurally-defined data (CLEVR) and organic data (MNIST and Fashion-MNIST), we demonstrate that BAYES-PROBE can sample close to the specified prediction confidence target while remaining in the known distribution. In the experiments, we show how BAYES-PROBE can be used to synthesize ambivalent predictions, uncover in-distribution adversarial examples, and understand novel-class extrapolation and domain adaptation behaviours.

Acknowledgements

The authors would like to thank Alex Lew, Marco Cusumano-Towner, Christian Muise, and Hendrik Strobel for fruitful discussions, and James Tompkin for comments on an earlier draft.

References

- Adebayo, J., Gilmer, J., Muelly, M., Goodfellow, I., Hardt, M., and Kim, B. Sanity checks for saliency maps. In *Advances in Neural Information Processing Systems*, pp. 9505–9515, 2018.
- Amir, O., Doshi-Velez, F., and Sarne, D. Summarizing agent strategies. *Autonomous Agents and Multi-Agent Systems*, 33(5):628–644, 2019.
- Arjovsky, M., Bottou, L., Gulrajani, I., and Lopez-Paz, D. Invariant risk minimization. *arXiv preprint arXiv:1907.02893*, 2019.
- Athalye, A., Carlini, N., and Wagner, D. Obfuscated gradients give a false sense of security: Circumventing defenses to adversarial examples. *arXiv preprint arXiv:1802.00420*, 2018.
- Bau, D., Zhou, B., Khosla, A., Oliva, A., and Torralba, A. Network dissection: Quantifying interpretability of deep visual representations. In *Proceedings of the IEEE Conference on Computer Vision and Pattern Recognition*, pp. 6541–6549, 2017.
- Bingham, E., Chen, J. P., Jankowiak, M., Obermeyer, F., Pradhan, N., Karaletsos, T., Singh, R., Szerlip, P., Horsfall, P., and Goodman, N. D. Pyro: Deep Universal Probabilistic Programming. *Journal of Machine Learning Research*, 2018.
- Blundell, C., Cornebise, J., Kavukcuoglu, K., and Wierstra, D. Weight uncertainty in neural networks. In *Proceedings of the 32nd International Conference on International Conference on Machine Learning-Volume 37*, pp. 1613–1622. JMLR. org, 2015.
- Carlini, N. and Wagner, D. Towards evaluating the robustness of neural networks. In *2017 IEEE Symposium on Security and Privacy (SP)*, pp. 39–57. IEEE, 2017.
- Chen, C., Li, O., Tao, D., Barnett, A., Rudin, C., and Su, J. K. This looks like that: deep learning for interpretable image recognition. In *Advances in Neural Information Processing Systems*, pp. 8928–8939, 2019.
- Cusumano-Towner, M. F., Saad, F. A., Lew, A. K., and Mansinghka, V. K. Gen: A general-purpose probabilistic programming system with programmable inference. In *Proceedings of the 40th ACM SIGPLAN Conference on Programming Language Design and Implementation*, PLDI 2019, pp. 221–236, New York, NY, USA, 2019. ACM. ISBN 978-1-4503-6712-7. doi: 10.1145/3314221.3314642. URL <http://doi.acm.org/10.1145/3314221.3314642>.
- DeVries, T. and Taylor, G. W. Learning confidence for out-of-distribution detection in neural networks. *arXiv preprint arXiv:1802.04865*, 2018.
- Doshi-Velez, F. and Kim, B. Towards a rigorous science of interpretable machine learning. *arXiv preprint arXiv:1702.08608*, 2017.
- Etmann, C., Lunz, S., Maass, P., and Schönlieb, C.-B. On the connection between adversarial robustness and saliency map interpretability. In *ICML*, 2019.
- Gal, Y. and Ghahramani, Z. Dropout as a bayesian approximation: Representing model uncertainty in deep learning. In *international conference on machine learning*, pp. 1050–1059, 2016.
- Ghorbani, A., Abid, A., and Zou, J. Interpretation of neural networks is fragile. In *Proceedings of the AAAI Conference on Artificial Intelligence*, volume 33, pp. 3681–3688, 2019a.
- Ghorbani, A., Wexler, J., and Kim, B. Automating interpretability: Discovering and testing visual concepts learned by neural networks. *arXiv preprint arXiv:1902.03129*, 2019b.
- Gilmer, J., Adams, R. P., Goodfellow, I., Andersen, D., and Dahl, G. E. Motivating the rules of the game for adversarial example research. *arXiv preprint arXiv:1807.06732*, 2018.
- Goodfellow, I. J., Shlens, J., and Szegedy, C. Explaining and harnessing adversarial examples. *arXiv preprint arXiv:1412.6572*, 2014.
- Guo, C., Pleiss, G., Sun, Y., and Weinberger, K. Q. On calibration of modern neural networks. In *Proceedings of the 34th International Conference on Machine Learning-Volume 70*, pp. 1321–1330. JMLR. org, 2017.
- Hayes, B. and Shah, J. A. Improving robot controller transparency through autonomous policy explanation. In *2017 12th ACM/IEEE International Conference on Human-Robot Interaction (HRI)*, pp. 303–312. IEEE, 2017.
- Hendrycks, D. and Gimpel, K. A baseline for detecting misclassified and out-of-distribution examples in neural networks. *arXiv preprint arXiv:1610.02136*, 2016.
- Hendrycks, D. and Gimpel, K. A baseline for detecting misclassified and out-of-distribution examples in neural networks. *Proceedings of International Conference on Learning Representations*, 2017.

- Hoffman, M. D. and Gelman, A. The no-u-turn sampler: adaptively setting path lengths in hamiltonian monte carlo. *Journal of Machine Learning Research*, 15(1):1593–1623, 2014.
- Huang, S. H., Held, D., Abbeel, P., and Dragan, A. D. Enabling robots to communicate their objectives. *Autonomous Robots*, 43(2):309–326, 2019.
- Johnson, J., Hariharan, B., van der Maaten, L., Fei-Fei, L., Zitnick, C. L., and Girshick, R. Clevr: A diagnostic dataset for compositional language and elementary visual reasoning. In *CVPR*, 2017.
- Kim, B., Rudin, C., and Shah, J. A. The bayesian case model: A generative approach for case-based reasoning and prototype classification. In *Advances in Neural Information Processing Systems*, pp. 1952–1960, 2014.
- Kim, B., Wattenberg, M., Gilmer, J., Cai, C., Wexler, J., Viegas, F., and Sayres, R. Interpretability beyond feature attribution: Quantitative testing with concept activation vectors (tcav). *arXiv preprint arXiv:1711.11279*, 2017.
- Kindermans, P.-J., Hooker, S., Adebayo, J., Alber, M., Schütt, K. T., Dähne, S., Erhan, D., and Kim, B. The (un) reliability of saliency methods. In *Explainable AI: Interpreting, Explaining and Visualizing Deep Learning*, pp. 267–280. Springer, 2019.
- Koh, P. W. and Liang, P. Understanding black-box predictions via influence functions. In *Proceedings of the 34th International Conference on Machine Learning-Volume 70*, pp. 1885–1894. JMLR. org, 2017.
- Lee, K., Lee, H., Lee, K., and Shin, J. Training confidence-calibrated classifiers for detecting out-of-distribution samples, 2017.
- Li, B., Chen, C., Wang, W., and Carin, L. Second-order adversarial attack and certifiable robustness. *arXiv preprint arXiv:1809.03113*, 2018a.
- Li, O., Liu, H., Chen, C., and Rudin, C. Deep learning for case-based reasoning through prototypes: A neural network that explains its predictions. In *Thirty-Second AAAI Conference on Artificial Intelligence*, 2018b.
- Liang, S., Li, Y., and Srikant, R. Principled detection of out-of-distribution examples in neural networks. *arXiv preprint arXiv:1706.02690*, 2017.
- Lipton, Z. C. The mythos of model interpretability. *Queue*, 16(3):31–57, 2018.
- Long, M., Cao, Y., Wang, J., and Jordan, M. I. Learning transferable features with deep adaptation networks. *arXiv preprint arXiv:1502.02791*, 2015.
- Lundberg, S. M. and Lee, S.-I. A unified approach to interpreting model predictions. In *Advances in neural information processing systems*, pp. 4765–4774, 2017.
- Ma, L., Juefei-Xu, F., Zhang, F., Sun, J., Xue, M., Li, B., Chen, C., Su, T., Li, L., Liu, Y., et al. Deepgauge: Multi-granularity testing criteria for deep learning systems. In *Proceedings of the 33rd ACM/IEEE International Conference on Automated Software Engineering*, pp. 120–131, 2018.
- Maaten, L. v. d. and Hinton, G. Visualizing data using t-sne. *Journal of machine learning research*, 9(Nov): 2579–2605, 2008.
- Neal, R. M. et al. Mcmc using hamiltonian dynamics. *Handbook of markov chain monte carlo*, 2(11):2, 2011.
- Netzer, Y., Wang, T., Coates, A., Bissacco, A., Wu, B., and Ng, A. Y. Reading digits in natural images with unsupervised feature learning. 2011.
- Nguyen, A., Yosinski, J., and Clune, J. Deep neural networks are easily fooled: High confidence predictions for unrecognizable images. In *Proceedings of the IEEE conference on computer vision and pattern recognition*, pp. 427–436, 2015.
- Odena, A., Olsson, C., Andersen, D., and Goodfellow, I. TensorFuzz: Debugging neural networks with coverage-guided fuzzing. In Chaudhuri, K. and Salakhutdinov, R. (eds.), *Proceedings of the 36th International Conference on Machine Learning*, volume 97 of *Proceedings of Machine Learning Research*, pp. 4901–4911, Long Beach, California, USA, 09–15 Jun 2019. PMLR. URL <http://proceedings.mlr.press/v97/odena19a.html>.
- Olah, C., Mordvintsev, A., and Schubert, L. Feature visualization. *Distill*, 2017. doi: 10.23915/distill.00007. <https://distill.pub/2017/feature-visualization>.
- Pei, K., Cao, Y., Yang, J., and Jana, S. Deepxplore: Automated whitebox testing of deep learning systems. In *proceedings of the 26th Symposium on Operating Systems Principles*, pp. 1–18, 2017.
- Peng, X. B., Andrychowicz, M., Zaremba, W., and Abbeel, P. Sim-to-real transfer of robotic control with dynamics randomization. In *2018 IEEE international conference on robotics and automation (ICRA)*, pp. 1–8. IEEE, 2018.
- Ribeiro, M. T., Singh, S., and Guestrin, C. ” why should i trust you?” explaining the predictions of any classifier. In *Proceedings of the 22nd ACM SIGKDD international conference on knowledge discovery and data mining*, pp. 1135–1144, 2016.

- Rudin, C. Stop explaining black box machine learning models for high stakes decisions and use interpretable models instead. *Nature Machine Intelligence*, 1(5):206–215, 2019.
- Simonyan, K., Vedaldi, A., and Zisserman, A. Deep inside convolutional networks: Visualising image classification models and saliency maps. *CoRR*, abs/1312.6034, 2013.
- Slack, D., Hilgard, S., Jia, E., Singh, S., and Lakkaraju, H. How can we fool lime and shap? adversarial attacks on post hoc explanation methods. *arXiv preprint arXiv:1911.02508*, 2019.
- Szegedy, C., Zaremba, W., Sutskever, I., Bruna, J., Erhan, D., Goodfellow, I., and Fergus, R. Intriguing properties of neural networks, 2013.
- Tan, J., Zhang, T., Coumans, E., Iscen, A., Bai, Y., Hafner, D., Bohez, S., and Vanhoucke, V. Sim-to-real: Learning agile locomotion for quadruped robots. *arXiv preprint arXiv:1804.10332*, 2018.
- Thulasidasan, S., Chennupati, G., Bilmes, J. A., Bhattacharya, T., and Michalak, S. On mixup training: Improved calibration and predictive uncertainty for deep neural networks. In *Advances in Neural Information Processing Systems*, pp. 13888–13899, 2019.
- Tobin, J., Fong, R., Ray, A., Schneider, J., Zaremba, W., and Abbeel, P. Domain randomization for transferring deep neural networks from simulation to the real world. In *2017 IEEE/RSJ international conference on intelligent robots and systems (IROS)*, pp. 23–30. IEEE, 2017.
- Tzeng, E., Hoffman, J., Zhang, N., Saenko, K., and Darrell, T. Deep domain confusion: Maximizing for domain invariance. *arXiv preprint arXiv:1412.3474*, 2014.
- Tzeng, E., Hoffman, J., Saenko, K., and Darrell, T. Adversarial discriminative domain adaptation. In *Proceedings of the IEEE Conference on Computer Vision and Pattern Recognition*, pp. 7167–7176, 2017.
- Vernekar, S., Gaurav, A., Abdelzad, V., Denouden, T., Salay, R., and Czarnecki, K. Out-of-distribution detection in classifiers via generation. *arXiv preprint arXiv:1910.04241*, 2019.
- Wicker, M., Huang, X., and Kwiatkowska, M. Feature-guided black-box safety testing of deep neural networks. In *International Conference on Tools and Algorithms for the Construction and Analysis of Systems*, pp. 408–426. Springer, 2018.
- Xiao, H., Rasul, K., and Vollgraf, R. Fashion-mnist: a novel image dataset for benchmarking machine learning algorithms. *arXiv preprint arXiv:1708.07747*, 2017.
- Zeiler, M. D. and Fergus, R. Visualizing and understanding convolutional networks. In *European conference on computer vision*, pp. 818–833. Springer, 2014.

Supplementary Materials

7 Network Architecture for MNIST & Fashion-MNIST

For all experiments on MNIST and Fashion-MNIST, the VAE architecture is shown in Table 2 (left), and the GAN architecture is shown in Table 2 (right). For all experiments on MNIST and Fashion-MNIST except for the domain adaptation analysis, the classifier architecture is shown in Table 3 (left). The classifier used in the domain adaptation analysis is the LeNet architecture, following the provided source code, shown in Table 3 (right). All experiments are performed with a single NVIDIA GeForce 1080 GPU.

Encoder input: $28 \times 28 \times 1$	Input: 5 (latent dimension)
Flatten	Reshape $1 \times 1 \times 5$
Fully-connected 784×400	Conv-transpose: 512 filters, size= 4×4 , stride = 1
ReLU	Batch-norm, ReLU
Mean: Fully-connected 400×5	Conv-transpose: 256 filters, size= 4×4 , stride = 2
Log-variance: Fully-connected 400×5	Batch-norm, ReLU
Decoder input: 5 (latent dimension)	Conv-transpose: 128 filters, size= 4×4 , stride = 2
Fully-connected 5×400	Batch-norm, ReLU
ReLU	Conv-transpose: 64 filters, size= 4×4 , stride = 2
Fully-connected 400×784	Batch-norm, ReLU
Reshape $28 \times 28 \times 1$	Conv-transpose: 1 filters, size= 1×1 , stride = 1
Sigmoid	Sigmoid

Table 2: Left: VAE architecture; right: GAN architecture.

Input: $28 \times 28 \times 1$	Input: $28 \times 28 \times 1$
Conv: 32 filters, size = 3×3 , stride = 1	Conv: 20 filters, size = 5×5 , stride = 1
ReLU	ReLU
Conv: 64 filters, size = 3×3 , stride = 1	Max-pool, size = 2×2
Drop-out, prob = 0.25	Conv: 50 filters, size = 5×5 , stride = 1
Max-pool, size = 2×2	ReLU
Flatten	Max-pool, size = 2×2
Fully-connected 9216×128	Flatten
ReLU	Fully-connected 800×500
Drop-out, prob = 0.5	ReLU
Fully-connected 128×10	Fully-connected 500×10
Soft-max	Soft-max

Table 3: Left: classifier architecture in experiments other than domain adaptation analysis; right: LeNet classifier architecture in domain adaptation analysis (used in the code released by the authors).

8 Fully Ambiguous Examples

We consider an additional target prediction class, corresponding to fully ambiguous examples.

For this case, we set the prediction target to be: $\mathbf{p}_i = 1/L, i \in \{1, \dots, L\}$. In this case, the classifier should be equally ambivalent in prediction across all classes. Note that it is unlikely that a well-trained model can admit realistic examples with totally ambivalent prediction, but this can still be a useful diagnostic test to run. For this case:

$$u|\mathbf{x} \sim \text{No}(\max_i f(\mathbf{x})_i - \min_j f(\mathbf{x})_j, \sigma^2), \tag{16}$$

$$u^* = 0, \tag{17}$$

where σ is a hyper-parameter.

Figure 12 presents samples with uniform prediction confidence, as generated by a VAE model. While the actual prediction does indeed match the uniform target, the images are blurry. We believe this blur is due to the classifier not being susceptible to producing fully ambiguous predictions on realistic, sharp images.

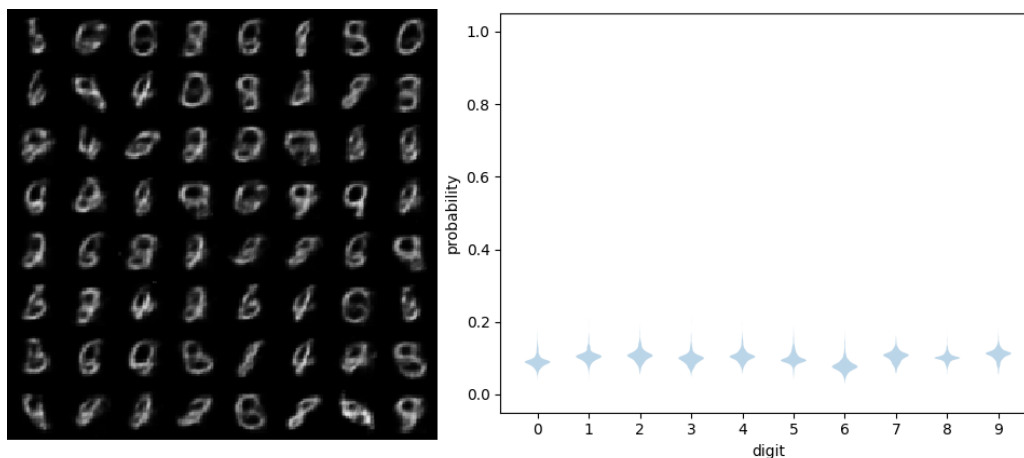


Figure 12: MNIST samples with fully ambiguous predictions, with corresponding violin plot of confidence.

9 MNIST and Fashion-MNIST Expanded Results

9.1 In-Distribution Adversarial Examples

Figure 13 shows additional samples and violin plots for in-distribution adversarial examples for MNIST class.

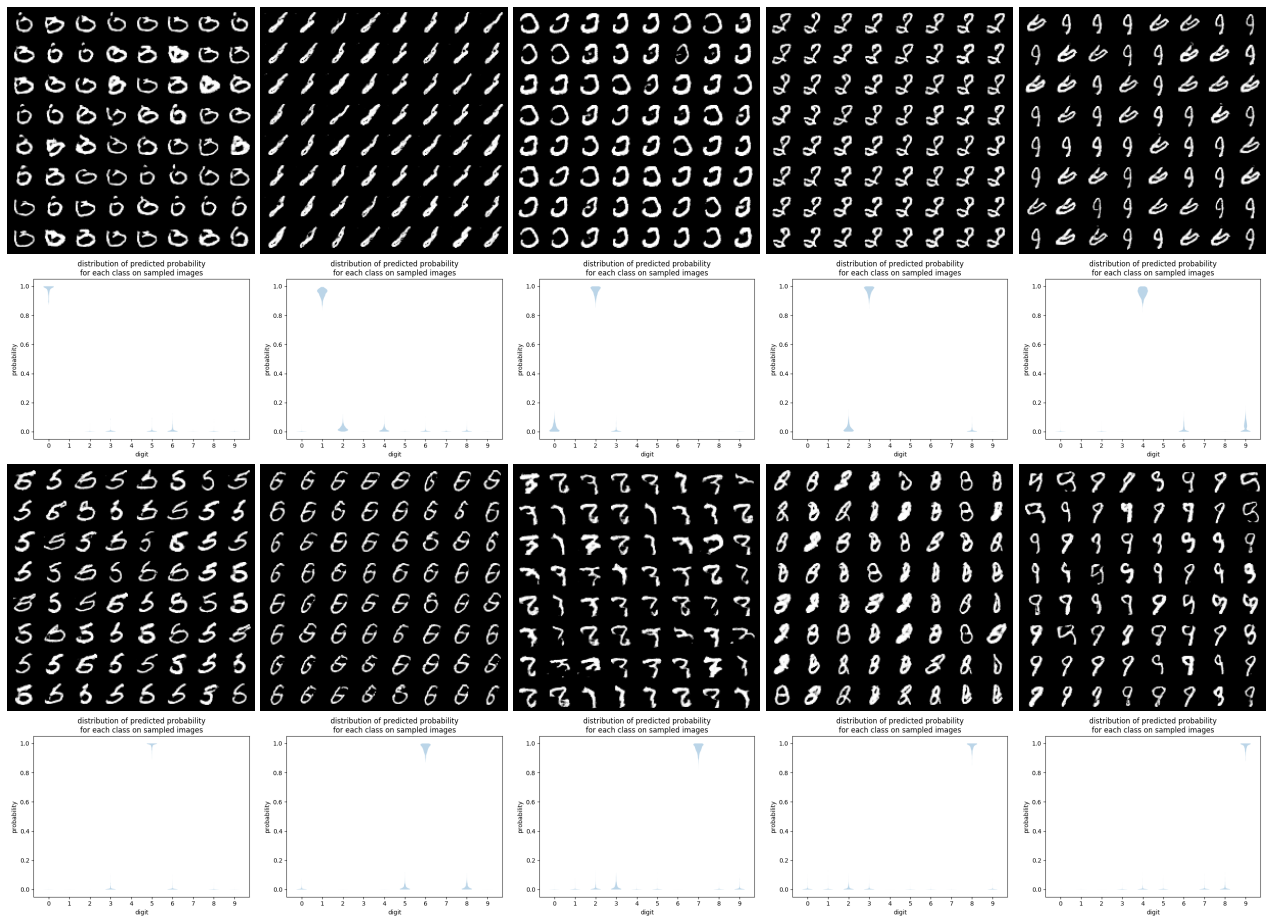


Figure 13: Additional samples and violin plots for in-distribution adversarial examples. Top two rows: digit 0-4; bottom two rows: digit 5-9.

Figure 14 shows additional samples and violin plots for in-distribution adversarial examples for Fashion-MNIST class. Sampling for the trouser class failed with 4000 samples.

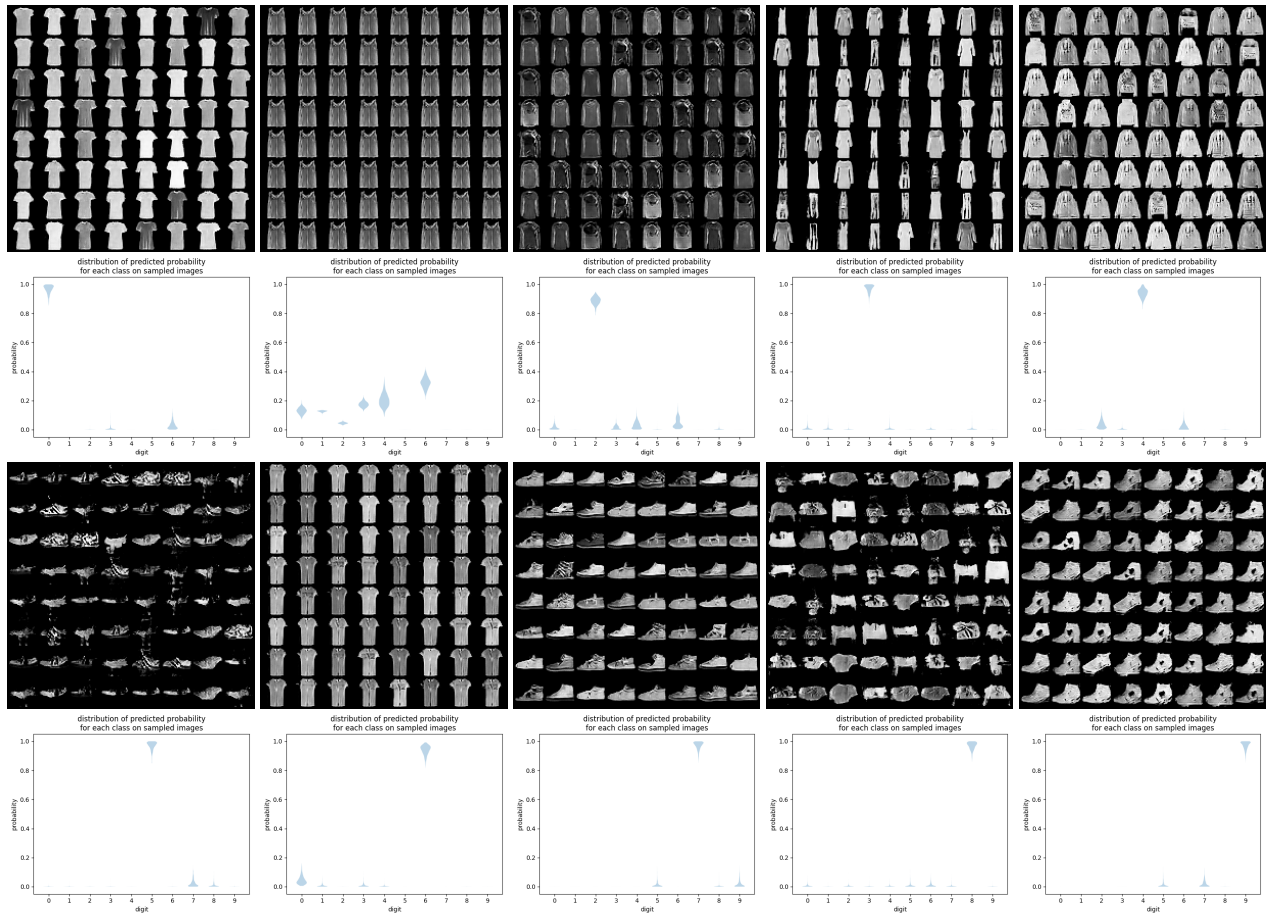


Figure 14: Additional samples and violin plots for in-distribution adversarial examples. Top two rows: T-shirt, trousers (sample failure), pullover, dress, coat; bottom two rows: sandal, shirt, sneaker, bag, ankle boot.

9.2 Novel-Class Extrapolation

Figure 15 shows additional samples and violin plots for novel-class extrapolation on MNIST. The classifier is trained on digit 0, 1, 3, 6 and 9, and tested on images generated by a GAN trained on digit 2, 4, 5, 7 and 8.

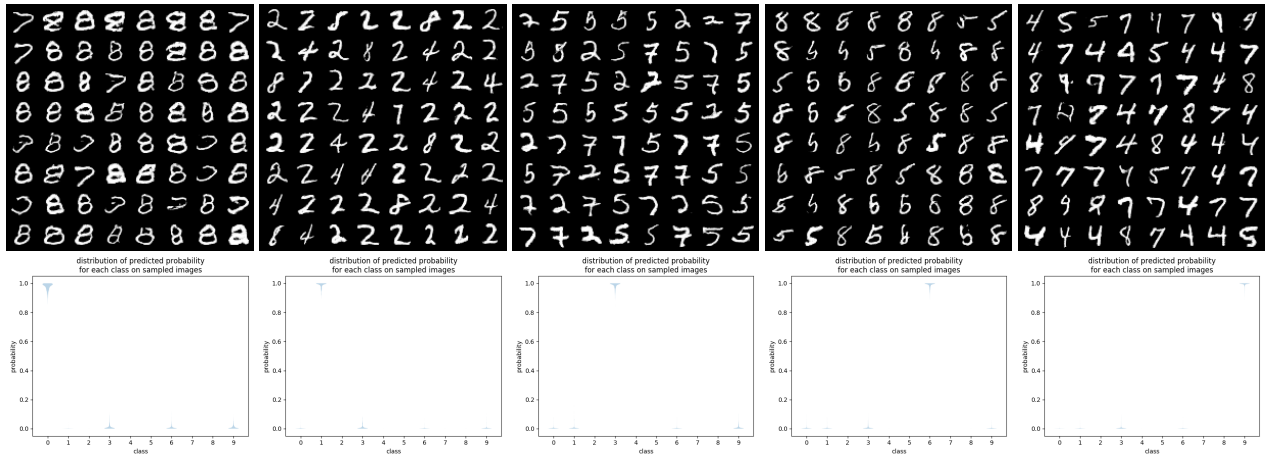


Figure 15: Additional samples and violin plots for novel-class extrapolation. Classifier classes are digit 0, 1, 3, 6 and 9, in that order.

Figure 16 shows additional samples and violin plots for novel-class extrapolation on Fashion-MNIST. The classifier is trained on pullover, dress, sandal, shirt and ankle boot, and tested on images generated by a GAN trained on T-shirt, trousers, coat, sneaker and bag.

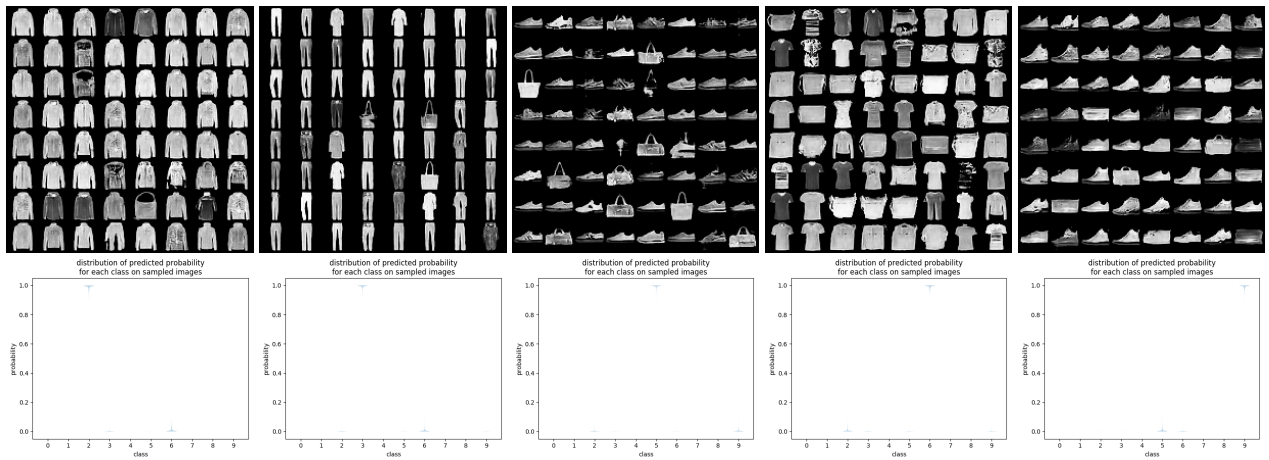


Figure 16: Additional samples and violin plots for novel-class extrapolation. Classifier classes are pullover, dress, sandal, shirt and ankle boot, in that order.

9.3 Domain Adaptation

Figure 17 shows additional samples and violin plots for the baseline model in the domain adaptation analysis. Top two rows are for digit 0-4, and bottom two rows are for digit 5-9.

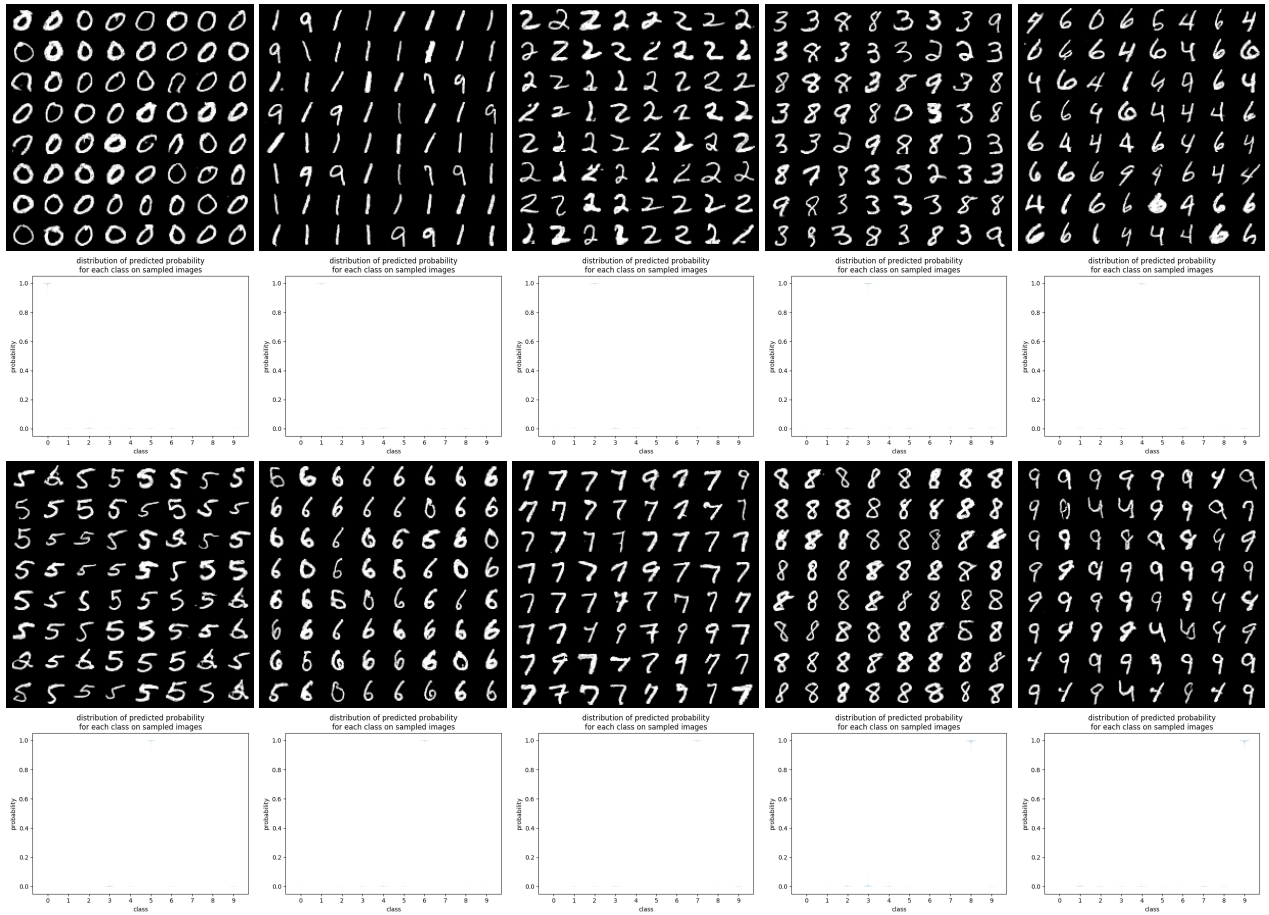


Figure 17: High confident MNIST samples generated for each class as predicted by the baseline model trained on SVHN dataset.

Figure 18 shows additional samples and violin plots for the adversarial discriminative domain adaptation (ADDA) model in the domain adaptation analysis. Top two rows are for digit 0-4, and bottom two rows are for digit 5-9.

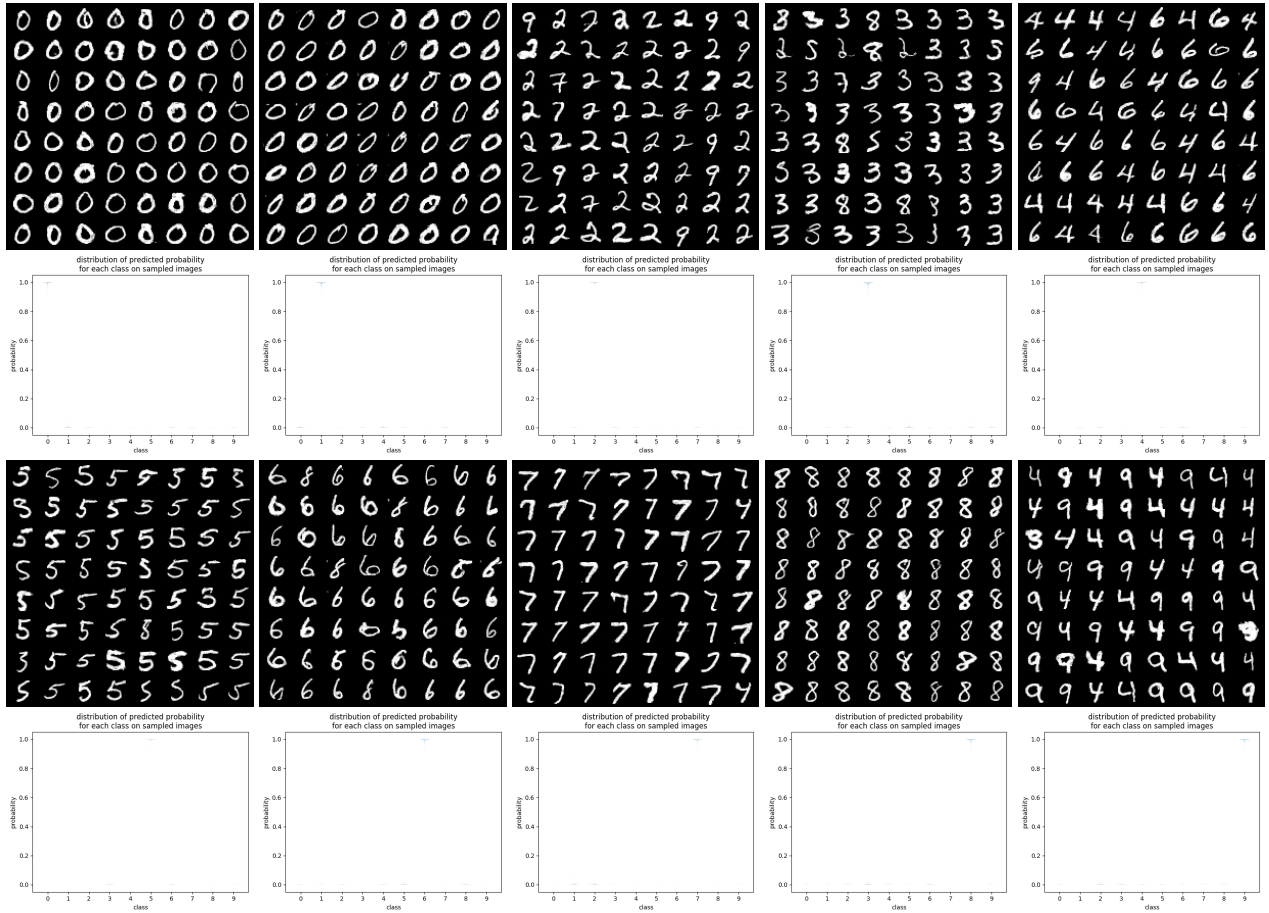


Figure 18: High confident MNIST samples generated for each class as predicted by the ADDA model trained on SVHN dataset.

10 CLEVR Expanded Results

10.1 In-Distribution Adversarial Examples

Figure 19 shows additional in-distribution adversarial examples for CLEVR. For each target (e.g. “1 Cube”), we revoked the ability of the generator to produce objects belonging to the target class (e.g., no cubes). Using the pretrained classifier, we then ran 20 inference trials.



Figure 19: Sampled in-distribution adversarial examples and their associated prediction confidences. For each target constraint (e.g., “1 Cube”), the generator is unable to produce examples from the target class (e.g., cubes). We run inference for 500 samples, 5 times for each target; we show the final accepted sample from each run.

10.2 Novel Class Extrapolation Examples

Figure 20 shows additional novel class extrapolation examples for CLEVR. Similar to the protocol for generating in-distribution adversarial examples, for each target (e.g. “1 Cube”), we revoked the ability of the generator to produce objects belonging to the target class (e.g., no cubes). We also introduced a new class to the generator, a cone. Using the pretrained classifier, we then ran 20 inference trials. Note that while the evaluation-time inference runs shown were successful (with low performance seen on Figure 20(p)), we did occasionally see inference failures. We uncovered these failures when attempting to satisfy unlikely constraints—for example, a scene composed exclusively of one type of object.

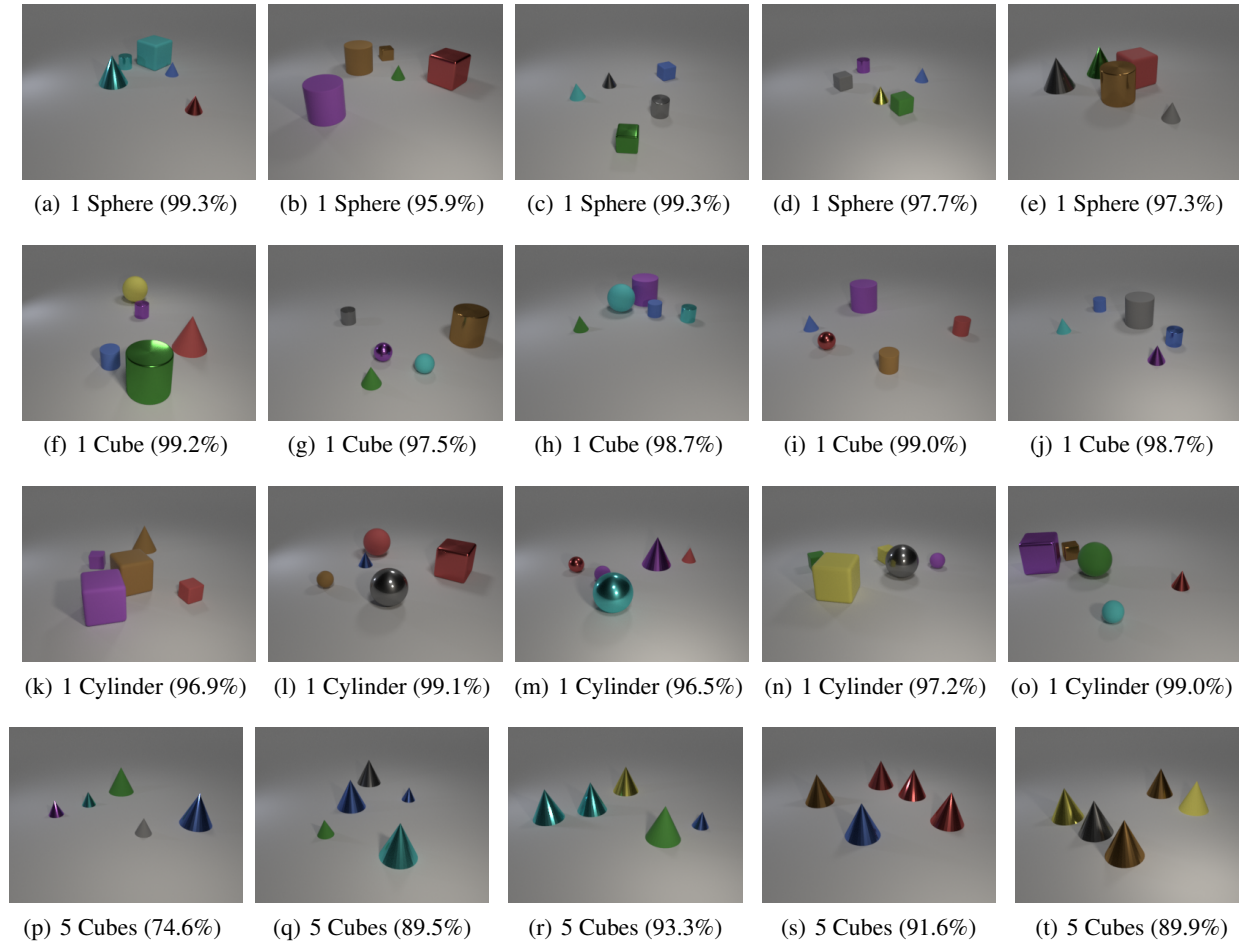


Figure 20: Sampled novel class extrapolation examples and their associated prediction confidences. As in the case of generating in-distribution adversarial examples, for each target constraint (e.g., “1 Cube”), we deprive the generator of the ability to produce examples from the target class (e.g., cubes). However, we also equip the data generator with the ability to generate a cone, a novel class which was not included in the training distribution. We run inference for 500 samples, 5 times for each target; we show the final accepted sample from each run. 20(n) is the only generated sample which does not include an object of the novel class.